

Variational Multiframe Restoration of Images Degraded by Noisy (Stochastic) Blur Kernels

Miyoun Jung, Antonio Marquina, and Luminita A. Vese*

Department of Mathematics, University of California,
Los Angeles, CA 90095, U.S.A.

Departamento de Matematica Aplicada, Universidad de Valencia,
Burjassot, Spain 46100.

Abstract. We wish to recover an original image u from several blurry-noisy versions f_k , called frames. We assume a more severe degradation model, in which the image u has been blurred by a noisy (stochastic) point spread function. We consider the problem of restoring the degraded image in a variational framework. Since the recovery of u from one single frame f is a highly ill-posed problem, we propose two minimization problems based on the multiframe approach introduced for image super-resolution by Marquina-Osher [28]. Several experimental results for grey-scale and color image restoration are shown, together with binary image segmentation of noisy-blurry data and restoration of static videos, illustrating that the proposed models give visually satisfactory results.

Keywords: image restoration, noisy blur kernel, energy minimization, regularization, multiframe model.

1 Introduction

Let Ω denote an open bounded set on which the image intensity function $u : \Omega \rightarrow R$ is defined. The standard linear degradation model for a blurry-noisy image f is given by $f = K * u + n$, where f is the observed image, K is a known linear and space-invariant blurring kernel, u is the ideal image, and n is additive noise, independent of u . One approach to the image restoration problem is within the variational framework, considering the minimization problem

$$\min_u \{ \Phi(f - K * u) + \Psi(|\nabla u|) \},$$

(as in [14, 15, 36]). Here, the functional $\Phi(\cdot)$ is a data-fidelity term that forces the smooth image $K * u$ to be close to the observed image f , while Ψ enforces a smoothness constraint on u , and can be seen as a regularizer in the ill-posed

* Research supported by the National Science Foundation Grants DMS-0312222, DMS-0714945, by a UCLA Faculty Research Grant 2009-2010, and by the Spanish Government Agency Grant DGI-CYT MTM2008-03597.

deconvolution problem. For example, for Gaussian noise n , a well-known edge-preserving image recovery model was proposed by Rudin-Osher [35, 36]: assuming $f \in L^2(\Omega)$, K linear and continuous on $L^2(\Omega)$, their model is

$$\min_u \left\{ \frac{\lambda}{2} \int_{\Omega} (f - K * u)^2 dx + \int_{\Omega} |\nabla u| dx \right\}, \quad (1)$$

where $\lambda > 0$ is a parameter and $TV(u) = \int_{\Omega} |\nabla u| dx$ is the total variation of $u \in W^{1,1}(\Omega) \subset BV(\Omega)$.

We consider in this paper a different degradation model with a noisy blur kernel inspired by [38], [40–42, 11, 19, 20, 1–4, 30]

$$f = (K + s) * u + n,$$

where K is a known blurring kernel (e.g. a Gaussian function), s is unknown additive Gaussian noise of zero mean (making K noisy), and n is another unknown additive Gaussian noise of zero mean. Both s and n are assumed to be statistically independent, and uncorrelated with u . Thus, the known blur kernel K is contaminated by noise s , producing a “stochastic point spread function”. The stochastically varying point spread function can be found in astronomy, e.g. atmospheric turbulence yielding a time-varying PSF, or in medical image, e.g. X-ray scattering.

Prior works to restore images distorted by random (or stochastic) point spread function were proposed: in the works [40–42, 11, 19, 20, 1–4, 30], generally, the linear PSF was assumed to contain a known deterministic mean and an additive random component with known statistics. Slepian [38] applied a Wiener filter to restore randomly blurred images. Ward-Saleh [40–42] presented a solution by modifying the Wiener filter and minimum variance unbiased estimator (both are one-dimensional), and the Backus-Gilbert filter. Combettes-Trussell [11] extended the method of projection onto convex sets and conventional constrained methods by incorporating the variations of the stochastic PSF as part of the a priori information. In [19], a geometrical mean filter that combined both the Wiener and the constrained least squares criteria [22] was developed. A robust non-parametric function estimation was introduced in [20], minimizing the maximal asymptotic variance as the error distribution vary over a suitable contamination neighborhood (long tailed noise), and a new technique based on Markov random field model was proposed in [1], being able to restore discontinuities. Moreover, Bilgen et al. [2–4] modified the Wiener filter and the constrained least-squares filter principles by incorporating the second-order statistics, such as correlations, about the randomness of the PSF. Mesarovic et al. [30] formulated the restoration problem as the solution of a perturbed set of linear equations, and the regularized constrained total least-squares method was used to solve this set of equations.

However, robust L^1 edge-preserving regularization techniques have not been applied to this image restoration problem. Furthermore, we explore here even more the degradation model, considering various (even large) sizes of blurring

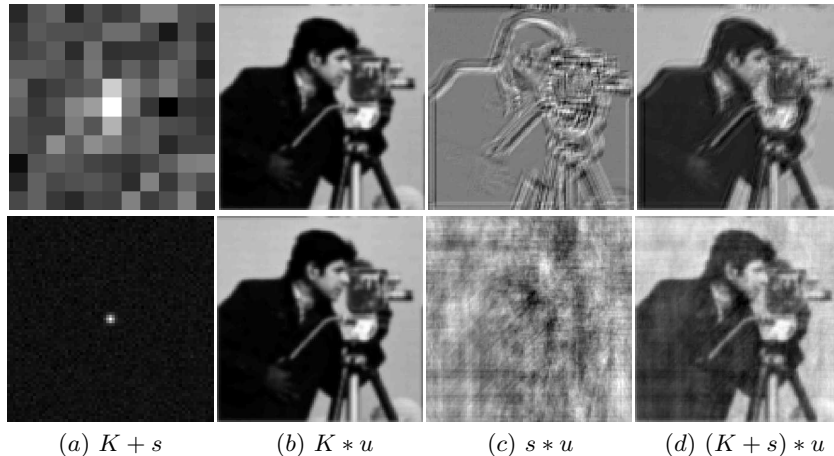


Fig. 1. The influence of the noise s present in the blurring kernel. Top: Gaussian blur kernel K of support 11×11 with $\sigma_b = 1$ and $s \sim N(0, 7^2)$. Bottom: Gaussian blur kernel K with support 71×71 with $\sigma_b = 1$ and $s \sim N(0, 0.8^2)$. PSNR: top (d) 20.0824, bottom (d) 20.9103.

kernels $(K + s)$ and extension to the multichannel (color) case and to static video restoration.

We first illustrate in Figure 1 this type of degradation on a real grey-scale image, in the case $n = 0$. We separate the degraded image $f = (K + s) * u$ shown in Fig. 1 (d) into two parts, $K * u$ and $s * u$, and we visualize $K * u$, $s * u$ in Fig. 1, to see how the noise s in the blurring kernel K influences the degraded image f . We use two blurring kernels $(K + s)$ with different support sizes, which leads to different degrees of degradation, perturbations or severe noise, that can be seen by looking at $s * u$ in Fig. 1. We notice that much of the information is kept in the $K * u$ term; thus, we propose here to consider $s * u$ as noise also (dependent on the unknown image u). Therefore, we reformulate the degradation model as

$$f = K * u + n_{s,u,n},$$

with a new noise term $n_{s,u,n} = s * u + n$. Because this reformulated degradation model looks like the standard one, we can attempt to apply the Rudin-Osher model [36] to recover u from f , as shown in Fig. 2 (b), and we compare these results with the case when s is known (Fig. 2 (a)). Of course, the recovery of u using the RO model, in the (nonrealistic) case when s is known, gives excellent results. However, as seen in Fig. 2 (b), the restored images using the RO model (1) with unknown s have visual artifacts and low PSNR, compared to the recovered images using the RO model with known s (replacing K by the true $K_s = K + s$ in (1)). Thus, the results in Fig. 2 (b) with unknown s are not satisfactory. Moreover, the blind deconvolution methods [44, 10, 21, 29] within the variational framework cannot be applied directly, since they assume that the unknown blur kernel is sufficiently smooth or at least piecewise smooth, which



Fig. 2. Recovered images from the degraded images in Fig. 1 (d) using (a) RO model with known s and one frame, using (b) RO model with unknown s and one frame. Top: recovery of Fig. 1 top (d). Bottom: recovery of Fig. 1 bottom (d). PSNR: top (a) 35.0097, (b) 23.0409, bottom (a) 36.5113, (b) 21.5140.

is not the case here. We conclude that it is very difficult to recover an image degraded by noisy blur kernel, as long as the noise s in the blurring kernel is unknown. For this reason, we make the problem slightly easier, by assuming that several frames (noisy-blurry versions of the same image u) are available, instead of only one, as presented next. The idea of using several degraded frames in the reconstruction of a single restored image is not new. Usually, low-resolution noisy-blurry frames are available to obtain a super-resolution image, as in [6], [33], [39, 32, 13], among other work. We mention that a preliminary version of this work has been presented at the International Conference in Image Processing ICIP 2009 [24].

2 Description of the proposed model

We borrow the idea of the multiframe model proposed for image super-resolution by Marquina-Osher [28]: we consider N given data frames (or a multiframe)

$$f_k = (K + s_k) * u + n_k,$$

with unknown noise terms s_k , n_k , $k = 1, 2, \dots, N$ of zero mean and variances σ_s^2 and σ_n^2 , respectively (e.g., N available data captured by a static video camera under bad atmospheric conditions and distortions caused by high temperatures and air turbulence). Then, similarly, we reformulate the degradation model $f_k = (K + s_k) * u + n_k$ as

$$f_k = K * u + n_{s_k, u, n_k}$$

with new unknown noise terms $n_{s_k, u, n_k} = s_k * u + n_k$, $k = 1, 2, \dots, N$. Hence, we formulate the general minimization problem with the above reformulated degradation model incorporating a multiframe

$$\min_u \left\{ \sum_{k=1}^N \Phi(f_k - K * u) + \Psi(|\nabla u|) \right\}$$

where Φ and Ψ define the fidelity and regularizing terms respectively. We will take advantage of the following known property [18], used here as follows: if we define at any point x

$$g = \frac{1}{N} \sum_{k=1}^N f_k = K * u + \left(\frac{1}{N} \sum_{k=1}^N s_k \right) * u + \left(\frac{1}{N} \sum_{k=1}^N n_k \right),$$

recalling that the noise terms s_k and n_k are of zero mean and uncorrelated with u , then it follows that

$$E\{g(x)\} = K * u(x),$$

where $E\{g(x)\}$ is the expected value of g . The variance of $g - K * u$, $\sigma_{g(x) - K * u(x)}^2$ at x is expressed as:

$$\begin{aligned} \sigma_{g(x) - K * u(x)}^2 &= E\{(g(x) - K * u(x))^2\} \\ &= E \left\{ \left(\left(\frac{1}{N} \sum_{k=1}^N s_k \right) * u(x) + \left(\frac{1}{N} \sum_{k=1}^N n_k \right) \right)^2 \right\} \\ &= E \left\{ \left(\left(\frac{1}{N} \sum_{k=1}^N s_k \right) * u(x) \right)^2 \right\} + E \left\{ \left(\frac{1}{N} \sum_{k=1}^N n_k(x) \right)^2 \right\} \\ &= \frac{1}{N} \sigma_{(s * u)(x)}^2 + \frac{1}{N} \sigma_{n(x)}^2 \end{aligned}$$

where $\sigma_{(s * u)(x)}^2$ and $\sigma_{n(x)}^2$ are the variances at x of $s * u$ and n respectively. Thus, the standard deviation at any point of this residual is

$$\sigma_{g(x) - K * u(x)} = \frac{1}{\sqrt{N}} \sqrt{\sigma_{(s * u)(x)}^2 + \sigma_{n(x)}^2}.$$

As N increases, the variability of the pixel values at each location x decreases. Because $E\{g(x)\} = K * u(x)$, this means that $g(x)$ approaches $K * u(x)$ as the number of noisy images used in the averaging process increases.

Now we propose two multiframe minimization problems based on the general multiframe model for grey-scale image restoration.

2.1 Multiframe/RO model

Assuming given $f_k \in L^2(\Omega)$, $k = 1, \dots, N$, we formulate a first minimization problem based on RO model [36],

$$\min_u \left\{ E(u) = \frac{\lambda}{2} \int_{\Omega} \sum_{k=1}^N \mu_k (f_k - K * u)^2 dx + \int_{\Omega} |\nabla u| dx \right\}, \quad (2)$$

where $\lambda > 0$ and $\mu_k > 0$ are given parameters with $\sum_{k=1}^N \mu_k = 1$. The associated Euler-Lagrange equation is given by

$$\frac{\partial E}{\partial u} = \lambda \left\{ \sum_{k=1}^N \mu_k \tilde{K} * (K * u - f_k) \right\} - \nabla \cdot \left(\frac{\nabla u}{|\nabla u|} \right) = 0,$$

which, due to the linearity of the blurring operator, is simplified to

$$\frac{\partial E}{\partial u} = \lambda \left\{ \tilde{K} * (K * u - \bar{f}) \right\} - \nabla \cdot \left(\frac{\nabla u}{|\nabla u|} \right) = 0,$$

where $\tilde{K}(x) = K(-x)$ and $\bar{f} = \sum_{k=1}^N \mu_k f_k$ is the weighted average of f_k 's. If we choose uniform weights $\mu_k = \frac{1}{N}$, then $\bar{f} = g$ the arithmetic mean of f_k 's. Following [28], we also consider different weights $\mu_k = \frac{TV(f_k)}{\sum_{k=1}^N TV(f_k)}$, thus we call \bar{f} the TV-mean of f_k 's in this case. We note that the PSNR values (peak signal-to-noise ratio computed using the true image u) for \bar{f} and for the arithmetic mean $g = \sum_{k=1}^N \frac{1}{N} f_k$ are larger than the PSNR for each f_k . However, both TV-mean and arithmetic mean are still blurry versions of the unknown image u .

2.2 Multiframe/Nonlocal TV model

We formulate a second minimization problem based on nonlocal methods. Starting with Buades et al. [8], nonlocal patch based methods [12] have been explored in many papers in image denoising, including [25], [16], [17], because these are well adapted to texture denoising while the standard denoising models working with local image information seem to consider texture as noise, which results in losing details. We consider the nonlocal total variation regularization proposed by Gilboa-Osher [16], [17], instead of the local one, using the notions of nonlocal gradient and nonlocal divergence inspired from graph-based methods [45]. Anisotropic smoothing is applied in both spatial and intensity neighborhoods [43].

Let $u : \Omega \rightarrow R$ be a function, and $w : \Omega \times \Omega \rightarrow R$ be a nonnegative and symmetric weight function. The nonlocal gradient vector $\nabla_w u : \Omega \times \Omega \rightarrow R$ is $(\nabla_w u)(x, y) := (u(y) - u(x))\sqrt{w(x, y)}$. Hence, the norm of the nonlocal gradient of u at $x \in \Omega$ is defined as

$$|\nabla_w u|(x) := \sqrt{\int_{\Omega} (u(y) - u(x))^2 w(x, y) dy}.$$

The nonlocal divergence $div_w \vec{v} : \Omega \rightarrow R$ of the vector $\vec{v} : \Omega \times \Omega \rightarrow R$ is defined as the adjoint of the nonlocal gradient,

$$(div_w \vec{v})(x) := \int_{\Omega} (v(x, y) - v(y, x))\sqrt{w(x, y)} dy.$$

Based on these nonlocal operators, Gilboa-Osher proposed the nonlocal TV regularizer (NLTV),

$$\int_{\Omega} |\nabla_w u| dx := \int_{\Omega} \sqrt{\int_{\Omega} (u(y) - u(x))^2 w(x, y) dy} dx,$$

which corresponds in the local case to $TV(u) = \int_{\Omega} |\nabla u| dx$.

Now we similarly propose a minimization problem with the nonlocal TV regularizer and multiframe model

$$\min_u \left\{ E(u) = \frac{\lambda}{2} \int_{\Omega} \sum_{k=1}^N \mu_k (f_k - K * u)^2 dx + \int_{\Omega} |\nabla_w u| dx \right\}, \quad (3)$$

where $\lambda > 0$ and $\mu_k > 0$ are given parameters with $\sum_{k=1}^N \mu_k = 1$. Similarly, we obtain the simplified Euler-Lagrange equation based only on the mean \bar{f} ,

$$\frac{\partial E}{\partial u} = \lambda \left\{ \tilde{K} * (K * u - \bar{f}) \right\} - \nabla_w \cdot \left(\frac{\nabla_w u}{|\nabla_w u|} \right) = 0,$$

where

$$\nabla_w \cdot \left(\frac{\nabla_w u}{|\nabla_w u|} \right) (x) = \int_{\Omega} (u(y) - u(x)) w(x, y) \left[\frac{1}{|\nabla_w u|(y)} + \frac{1}{|\nabla_w u|(x)} \right] dy.$$

Furthermore, in practice, we use the weight function w at $(x, y) \in \Omega \times \Omega$ depending on an image $q : \Omega \rightarrow R$,

$$w_q(x, y) = \exp \left(-\frac{d_a(q(x), q(y))}{h^2} \right),$$

$$d_a(q(x), q(y)) = \int_{R^2} G_a(t) |q(x+t) - q(y+t)|^2 dt,$$

where d_a is the patch distance, G_a is the Gaussian kernel with standard deviation a determining the patch size, and h is the filtering parameter which corresponds to the noise level [8]. The weight function $w(x, y)$ gives the similarity of the intensity values as well as of image features between two pixels x and y in the image q , which will be defined in Section 2.3. Note that, with a given noisy data (no blur), the weights w are usually computed from the data itself. Recently for image deblurring and denoising, Lou et al. [26] used a preprocessed image q to define the weights w , obtained by applying the Wiener filter to the blurry-noisy data. Also, in practice, for a fixed pixel $x \in \Omega$, we use a search window $S(x) = \{y \in \Omega : |x - y| \leq r\}$ to compute $w(x, y)$ instead of Ω .

2.3 Extension to multichannel data

Now we consider the multichannel (color) degradation models defined as

- (A) $f^i = (K + s) * u^i + n^i, \quad i \in \{r, g, b\}$ or
- (B) $f^i = (K + s^i) * u^i + n^i, \quad i \in \{r, g, b\}$

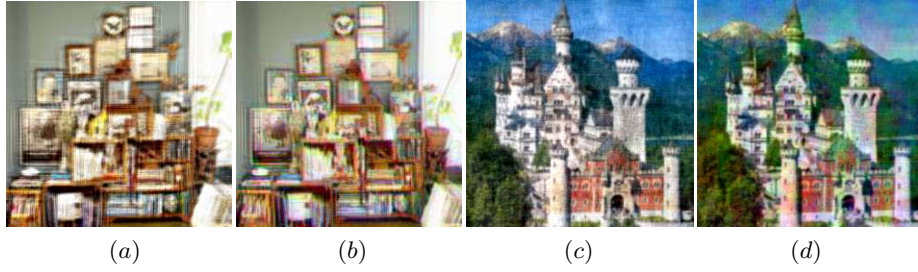


Fig. 3. Degraded images $(K + s) * u$, (a)-(b): with Gaussian blur kernel K of support 22×22 with $\sigma_b = 1$, $s \sim N(0, 4^2)$, (c)-(d): with Gaussian blur kernel K of support 176×176 with $\sigma_b = 1$, $s \sim N(0, 0.4^2)$. (a), (c): type A (b), (d): type B. PSNR: (a) 16.8572, (b) 17.3500, (c) 18.0546, (d) 17.6463.

which are illustrated in Fig. 3 on real images, in the case $n^i = 0$. We observe that even though the degraded images (a) and (b) (or (c) and (d)) by the above degradation models (A) and (B) respectively look different, the type of degradations are similar in the sense that the data (a) and (b) (or (c) and (d)) with a small size of blur kernel K (or a large size of K) produce perturbations (or severe noise) like in the grey-scale case. Thus, we again use the multiframe idea for the multichannel version.

Assuming N given data frames (a multiframe), we reformulate the degradation models as

$$(A.2) \quad f_k^i = (K + s_k) * u^i + n_k^i = K * u^i + n_{s_k, u^i, n_k^i}^i, \quad i \in \{r, g, b\}$$

$$(B.2) \quad f_k^i = (K + s_k^i) * u^i + n_k^i = K * u^i + n_{s_k^i, u^i, n_k^i}^i, \quad i \in \{r, g, b\}$$

where s_k (or s_k^i) and n_k^i , $k = 1, 2, \dots, N$, are unknown noise terms of zero mean and variances σ_s^2 and σ_n^2 respectively, $n_{s_k, u, n_k}^i = s_k * u^i + n_k^i$, and $n_{s_k^i, u, n_k}^i = s_k^i * u^i + n_k^i$. Hence, we end up with the same degradation models (A.2) and (B.2) considering both n_{s_k, u, n_k}^i and $n_{s_k^i, u, n_k}^i$ as noises, which leads to a similar minimization problem:

MULTIFRAME/RO MODEL

$$\min_u \left\{ E(u) = \frac{\lambda}{2} \int_{\Omega} \sum_{k=1}^N \mu_k \left(\sum_{i=r, g, b} (f_k^i - K * u^i)^2 \right) dx + \int_{\Omega} \|\nabla u\| dx \right\}, \quad (4)$$

where $\lambda > 0$, $\mu_k > 0$ are given parameters with $\sum_{k=1}^N \mu_k = 1$, $\|\nabla u\|$ is defined by

$$\|\nabla u\| = \sqrt{\sum_{i=r, g, b} [(u_x^i)^2 + (u_y^i)^2]},$$

and $\int_{\Omega} \|\nabla u\| dx$ is a generalization of TV regularization to color images with coupled channels [5, 7]. Using the linearity of K , we obtain the simplified associated Euler-Lagrange equations given by

$$\frac{\partial E}{\partial u^i} = \lambda \left\{ \tilde{K} * (K * u^i - \bar{f}^i) \right\} - \nabla \cdot \left(\frac{\nabla u^i}{\|\nabla u\|} \right) = 0, \quad i \in \{r, g, b\}$$

where $\bar{f}^i = \sum_{k=1}^N \mu_k f_k^i$ is the weighted average of f_k^i for each $i \in \{r, g, b\}$ (i.e. $\bar{f} = \sum_{k=1}^N \mu_k f_k$ is the weighted average of f_k). Note that we use $\mu_k = \frac{\int_{\Omega} \|\nabla f_k\| dx}{\sum_{k=1}^N \int_{\Omega} \|\nabla f_k\| dx}$ corresponding to the TV-mean in Section 2.1. Moreover, \bar{f} is still a blurry version of the ideal color image u .

Similarly, we also formulate the color version of Multiframe/Nonlocal TV model by extending the scalar nonlocal operators to the vector-valued ones:

MULTIFRAME/NONLOCAL TV MODEL

$$\min_u \left\{ E(u) = \frac{\lambda}{2} \int_{\Omega} \sum_{k=1}^N \mu_k \left(\sum_{i=r,g,b} (f_k^i - K * u^i)^2 \right) dx + \int_{\Omega} \|\nabla_w u\| dx \right\}, \quad (5)$$

where $\lambda > 0$, $\mu_k > 0$ are given parameters with $\sum_{k=1}^N \mu_k = 1$, and $\|\nabla_w u\| : \Omega \rightarrow R$ is defined as

$$\|\nabla_w u\|(x) := \sqrt{\sum_{i=r,g,b} |\nabla u_w^i|^2(x)} := \sqrt{\sum_{i=r,g,b} \int_{\Omega} (u^i(y) - u^i(x))^2 w(x, y) dy}$$

with the weight function $w = w_q : \Omega \times \Omega \rightarrow R$ defined in Section 2.2, computed by the following patch distance

$$d_a(q(x), q(y)) = \int_{R^2} G_a(t) \|q(x+t) - q(y+t)\|^2 dt.$$

The Euler-Lagrange equations are also given based only on the means \bar{f}^i by

$$\frac{\partial E}{\partial u^i} = \lambda \left\{ \tilde{K} * (K * u^i - \bar{f}^i) \right\} - \nabla_w \cdot \left(\frac{\nabla_w u^i}{\|\nabla_w u\|} \right) = 0, \quad i \in \{r, g, b\}$$

where

$$\nabla_w \cdot \left(\frac{\nabla_w u^i}{\|\nabla_w u\|} \right) (x) = \int_{\Omega} (u^i(y) - u^i(x)) w(x, y) \left[\frac{1}{\|\nabla_w u\|(y)} + \frac{1}{\|\nabla_w u\|(x)} \right] dy.$$

We define now q , to be used in the computation of weights w . First, we simply use the mean \bar{f} as q because even though $\bar{f} \approx K * u$ is a blurry image, it still can keep well the geometrical configurations of the original image u . Second, we use another image, a sharper image \bar{g} , instead of \bar{f} :

$$\bar{g} = \text{deconvlucy}(\bar{f}, K, \alpha),$$

Table 1. ALGORITHM OF MULTIFRAME/NLTV MODEL

Data	we get a multiframe; $f_k, k = 1, 2, \dots, N$.
Weights	<ol style="list-style-type: none"> we obtain the weighted average \bar{f} of the multiple data; $\bar{f} = \sum_{k=1}^N \mu_k f_k$ with $\mu_k = \frac{ \nabla f_k }{\sum_{k=1}^N \nabla f_k }$ (grey-scale) or $\mu_k = \frac{\ \nabla f_k\ }{\sum_{k=1}^N \ \nabla f_k\ }$ (color). we get a preprocessed image \bar{g} obtained by applying Lucy-Richardson algorithm to \bar{f}; $\bar{g} = \text{deconvlucy}(\bar{f}, K, \alpha)$. we use either \bar{f} or a preprocessed image \bar{g} to construct weight function $w = w(x, y)$; for fixed $x \in \Omega$, we compute weights $w(x, y)$, defined in the section 2.2, for $y \in S(x)$, where $S(x)$ is a search window centered at x.
Minimization	<ol style="list-style-type: none"> Input $f_k, \mu_k (k = 1, 2, \dots, N), K$, and a fixed parameter λ. Minimize the energy functional to restore u; $u = \operatorname{argmin} E(u)$ where $E(u)$ is given in the section 2.2 or section 2.3 ((3),(5)).

where `deconvlucy` is Lucy-Richardson deconvolution method [27, 34], an iterative procedure for recovering an ideal image from the blurred image \bar{f} with a known point spread function K , and α is the number of iterations the `deconvlucy` function performs. Note that we in practice generate a data using `imfilter` in MATLAB:

either (1) $f_k = \text{imfilter}(u, K + s_k, 'circular', 'conv')$, $k = 1, 2, \dots, N$

or (2) $f_k = \text{imfilter}(u, K + s_k, 'symmetric', 'conv')$, $k = 1, 2, \dots, N$.

Here, for the second case (2), if we apply `imfilter` directly to \bar{f} , then the generated image \bar{g} has some artifacts near the boundary that look like ringing effect.

To avoid this, we first expand the mean \bar{f} to \tilde{f} such as $\tilde{f} = \text{padarray}(\bar{f}, [m \ m], 'symmetric')$ and we apply `deconvlucy` to \tilde{f} producing \hat{g} , and then reduce \hat{g} again to the original size, which provides a preprocessed image \bar{g} for the data (2). We used $m = 10$, and for the first case (1), we apply `deconvlucy` directly to the \bar{f} . In practice, we use $q = \bar{f}$ for grey-scale images, and $q = \bar{f}$ or $q = \bar{g}$ for color images, so we compare the recovered images with $q = \bar{f}$ or $q = \bar{g}$.

2.4 Application to joint restoration and binary segmentation

Here we present another application of the multiframe idea, joint segmentation and restoration of a binary image degraded by a noisy blur kernel, from several frames. First, let $\phi : \Omega \rightarrow R$ be a level set function (usually a Lipschitz continuous function) whose zero level set represents the evolving curve

$C = \{x \in \Omega : \phi(x) = 0\}$ [31], [37], and define $f : \Omega \rightarrow R$ by the given data to be restored and segmented, assuming the degradation

$$\begin{aligned} f &= (K + s) * u + n \\ &= (K + s) * \left(c_1 H(\phi) + c_2 (1 - H(\phi)) \right) + n, \end{aligned}$$

which is an extension of the degradation model $f = K * \left(c_1 H(\phi) + c_2 (1 - H(\phi)) \right) + n$ proposed in [23] for joint denoising, deblurring and segmentation of a binary image u , with unknown constants c_1 , c_2 , and one-dimensional Heaviside function H .

Again, assuming N given data frames, we formulate the binary image segmentation and restoration minimization problem incorporating a multiframe:

$$\begin{aligned} \min_{c_1, c_2, \phi} \left\{ E(c_1, c_2, \phi) = \frac{1}{2} \int_{\Omega} \left(\sum_{l=1}^N \mu_l \left| f_l - K * \left(c_1 H(\phi) + c_2 (1 - H(\phi)) \right) \right|^2 \right) dx \right. \\ \left. + \lambda \int_{\Omega} |\nabla H(\phi)| dx \right\}, \end{aligned} \quad (6)$$

where $\lambda > 0$, $\mu_l > 0$ are given parameters with $\sum_{l=1}^N \mu_l = 1$.

We compute the Euler-Lagrange equations minimizing the energy E with respect to c_1 , c_2 , and ϕ . Using alternating minimization, keeping first ϕ fixed and minimizing the energy with respect to the unknown constants c_1 and c_2 , we obtain the following linear system of equations:

$$\begin{aligned} c_1 \int_{\Omega} k_1^2 dx + c_2 \int_{\Omega} k_1 k_2 dx &= \int \bar{f} k_1 dx, \\ c_1 \int_{\Omega} k_1 k_2 dx + c_2 \int_{\Omega} k_2^2 dx &= \int \bar{f} k_2 dx \end{aligned}$$

with the mean $\bar{f} = \sum_{l=1}^N \mu_l f_l$, $k_1 = K * H(\phi)$ and $k_2 = K * (1 - H(\phi))$. Note that the linear system has a unique solution because the determinant of the coefficient matrix is not zero due to the Cauchy-Schwartz inequality [23].

Keeping now the constants c_1 and c_2 fixed and minimizing the energy with respect to ϕ , we obtain the simplified Euler-Lagrange equation involving only the mean \bar{f} of given multiple frames

$$\begin{aligned} \frac{\partial E}{\partial \phi} &= \delta(\phi) \left[\left(\tilde{K} * \bar{f} - c_1 \tilde{K} * (K * H(\phi)) - c_2 \tilde{K} * (K * (1 - H(\phi))) \right) \cdot \right. \\ &\quad \left. (c_2 - c_1) - \mu \nabla \cdot \left(\frac{\nabla \phi}{|\nabla \phi|} \right) \right] = 0, \end{aligned}$$

where δ denotes the one-dimensional Dirac distribution (in practice, we substitute H and δ by smooth approximations, as in [9]).

2.5 Numerical approximations

Minimization of the proposed energy functionals $E(u)$ (or $E(c_1, c_2, \phi)$ with fixed c_1, c_2 from Section 2.4) is carried out using the Euler-Lagrange equations with homogeneous Neumann boundary conditions $\partial u / \partial \mathbf{n} = 0$ (or $\partial \phi / \partial \mathbf{n} = 0$), where \mathbf{n} is the exterior normal to the image boundary. We already presented the Euler-Lagrange equations $\partial E(u) / \partial u = 0$ and $\partial E(c_1, c_2, \phi) / \partial \phi = 0$ of the models (2)-(5) and (6) respectively, in the previous sections. Based on these Euler-Lagrange equations, we use the steepest gradient descent scheme,

$$\frac{\partial u}{\partial t} = -\frac{\partial E(u)}{\partial u}, \quad \text{or} \quad \frac{\partial \phi}{\partial t} = -\frac{\partial E(c_1, c_2, \phi)}{\partial \phi}.$$

The basic discretizations are presented next, separating the local and nonlocal cases.

MULTIFRAME/RO OR MULTIFRAME SEGMENTATION MODEL Let $u_{i,j}^\sigma$ denote the discretized version of $u^\sigma(x, y)$ with $(x, y) \in \Omega$ in channel σ ; $\sigma \in \{r, g, b\}$ for the multichannel case, but for the grey-scale case we replace u^σ by u . The forward and backward finite difference approximations of the derivatives $\partial u_{i,j}^\sigma / \partial x$ and $\partial u_{i,j}^\sigma / \partial y$ are respectively defined by

$$\Delta_\pm^x u_{i,j}^\sigma = \pm(u_{i\pm 1,j}^\sigma - u_{i,j}^\sigma), \quad \Delta_\pm^y u_{i,j}^\sigma = \pm(u_{i,j\pm 1}^\sigma - u_{i,j}^\sigma),$$

and the central finite difference approximation is

$$\Delta_c^x u_{i,j}^\sigma = \frac{u_{i+1,j}^\sigma - u_{i-1,j}^\sigma}{2}, \quad \Delta_c^y u_{i,j}^\sigma = \frac{u_{i,j+1}^\sigma - u_{i,j-1}^\sigma}{2}.$$

The discretization of $\|\nabla u\|^2$ was carried out using the central difference scheme

$$\|\nabla u\|^2 = \sum_{\sigma \in \{r, g, b\}} (\Delta_c^x u_{i,j}^\sigma)^2 + (\Delta_c^y u_{i,j}^\sigma)^2.$$

Terms of the form $\nabla \cdot (c(x, y) \nabla u^\sigma)$ were discretized using forward difference for the gradient and backward difference for the divergence

$$\nabla \cdot (c(x, y) \nabla u^\sigma) = \Delta_-^x (c(i, j) \Delta_+^x u_{i,j}^\sigma) + \Delta_-^y (c(i, j) \Delta_+^y u_{i,j}^\sigma).$$

MULTIFRAME/NLTV MODEL Let u_k^σ denote the value of a pixel k in the image ($1 \leq k \leq N$) with channel σ (i.e. the discretized version of $u^\sigma(x)$ defined on Ω), and let $p_{k,l}^\sigma$ be the discretized version of $p^\sigma(x, y)$ with $x, y \in \Omega$. $w_{k,l}$ is the sparsely discrete version of $w = w(x, y) : \Omega \times \Omega \rightarrow R$. We use the neighbors set $l \in N_k$ defined as $l \in N_k := \{l : w_{k,l} > 0\}$. Then we have ∇_{wd} and div_{wd} , the discretizations of ∇_w and div_w , defined respectively as [17]

$$\begin{aligned} \nabla_{wd}(u_k^\sigma) &:= (u_l^\sigma - u_k^\sigma) \sqrt{w_{k,l}}, \quad l \in N_k, \\ div_{wd}(p_{k,l}^\sigma) &:= \sum_{l \in N_k} (p_{k,l}^\sigma - p_{l,k}^\sigma) \sqrt{w_{k,l}}. \end{aligned}$$

Moreover, the magnitude of $p_{k,l}^\sigma$ at k is $|p^\sigma|_k = \sqrt{\sum_l (p_{k,l}^\sigma)^2}$, thus the discretization of $\|\nabla u_w\|^2(x)$ was done as

$$\|\nabla u_{wd}\|_k^2 = \sum_{\sigma \in \{r,g,b\}} |\nabla_{wd} u^\sigma|_k^2 = \sum_{\sigma \in \{r,g,b\}} \sum_l (u_l^\sigma - u_k^\sigma)^2 w_{k,l}.$$

We construct the weight function $w_{k,l}$, following the algorithm in [16]: for each pixel k , (1) take a patch B_k around a pixel k , compute the distances $(d_a)_{k,l}$ (a discretization of d_a) to all the patches B_l in the search window $l \in S(k)$, and construct the neighbors set N_k by taking the m most similar and the four nearest neighbors of the pixel k , (2) compute the weights $w_{k,l}$ defined in Section 2.2, $l \in N_k$ and set to zero all other connections ($w_{k,l} = 0, l \notin N_k$), (3) set $w_{k,l} = w_{l,k}, l \in N_k$. In all the examples, we used $m = 5$, so a maximum of up to $2m + 4$ neighbors for each pixel is allowed in our implementation, and we used 5×5 pixel patches with $a = 1$, a search window of size 11×11 . The complexity of computing the weights using this algorithm is $N \times Window_{size} \times (Patch_{size} \times Channal_{size} + \log m)$. Thus, in our color case, we need $121 \times (25 \times 3 + 2.5) \approx 9619$ operations per pixel. Most of the computation time is in this part.

3 Experimental results

We first test the proposed models (2)-(5) based on the multiframe approach, for the recovery of grey-scale and color images degraded by noisy blur kernel, using mostly 10 data frames (e.g. Fig. 4-14). We test on grey-scale images in Figures 4-7, and on color images in Figures 8-15, 17. As mentioned in Section 2.3, for Multiframe/NLTV model, we use the mean $q = \bar{f}$ in the grey-scale case, and a preprocessed image $q = \bar{g}$ or $q = \bar{f}$ in the color one to compute the weight function $w = w_q$. In Figures 11-14, we compared the recovered images using Multiframe/NLTV model (5) with different weight function $w = w_q; q = \bar{g} = \text{deconvlucy}(\bar{f}, \alpha)$ by varying α or $q = \bar{f}$. In Fig. 15, with different number of data frames k , we present the PSNR values of \bar{f} , the recovered images using the proposed multiframe models (4), (5) vs k . In Fig. 17, we test on a real color video, each frame being degraded by varying noisy blur kernels (i.e. $K + s_k$). At last, in Fig. 16, we test the proposed multiframe segmentation model (6) on severely degraded data.

In Fig. 4, we recover the two different degraded image types shown in Fig. 1 (d), having some perturbations or severe noise induced by the noise s_k in the blur kernel, using the proposed multiframe models (2), (3) with 10 frames. First, as expected, we observe that both models provide visually more satisfactory results than the one-frame RO model (1) (see Fig. 2 (b)), and much higher PSNR values. Moreover, Multiframe/NLTV model reduces the staircase effect appeared in the images recovered with Multiframe/RO model, and also gives higher PSNR values.

Similarly, in the case of the Barbara image in Fig. 5, containing texture, we can see that Multiframe/NLTV model produces again better recovered image,

especially by restoring well the texture, leading to higher PSNR than Multiframe/RO model. We also compare the results with the one-frame RO model (1) and the proposed multiframe models. Even though the degradation in f does not look severe, one frame model (1) suffers from recovering the image, still keeping some artifacts (e.g. on the lower part of the face) generated by the noise s . However, using the average of 10 noisy-blurry frames reduces very much the perturbations, and produces much better recovered images with the proposed multiframe models.

In Figures 6 and 7, we use the pill box kernel with the same radius $r = 2$ but $K + s$ of different supports, 31×31 in Fig. 6 and 71×71 in Fig. 7. As we have seen in the previous examples, the degraded image $f = (K + s) * u + n$ in Fig. 6 (one of the frames) corresponding to the small size of blurring kernel still has severe perturbations generated by the noise s , but the TV-mean \bar{f} reduces the perturbations a lot, which leads to satisfactory recovered images. Similarly, the image $f = (K + s) * u + n$ in Fig. 7 corresponding to the large size of blur kernel seems to have severe noise, that is also generated by the noise s , but the average \bar{f} reduces the noise leading to much higher PSNR, which results in a nice recovery of images.

In Figures 8-10, we recover the degraded color images by adding noise to the images (a)-(d), shown in Fig. 3 using `imfilter` function in MATLAB with Gaussian noise density d . First, as in the grey-scale case, we observe that the mean \bar{f} reduces the perturbations or noise produced by the noise $s * u$ a lot, improving both visual quality and PSNR, which also leads to good recovered images in both models (4), (5). In all examples, Multiframe/NLTV model provides larger PSNR than Multiframe/RO model even though both produce visually very similar results. But in the case of the Barbara image in Fig. 13, containing texture, Multiframe/NLTV model gives better visual quality and larger PSNR, by recovering texture better and with less artifacts on the face and hand. Moreover, despite some artifacts due to $s * u$ in the deblurred image \bar{g} (for example, \bar{g} in Fig. 8 includes some amplification of the perturbations induced by $s * u$), the recovered image using Multiframe/NLTV model with $q = \bar{g}$ doesn't include the artifacts, producing cleaner image.

In Figures 11-14, we compare the recovered images using Multiframe/NLTV model (5) with the weights $w = w_q$ based on different q . In Fig. 11, we recovered the degraded images in Fig. 10 with $q = \bar{g}$ by varying α . As seen both in Fig. 11 and in Fig. 12, as α increases, \bar{g} gets sharper, thus the PSNR value of the recovered image increases, with the same optimal λ . Note that each example through Figures 8-12 has the same optimal λ ; $\lambda = 0.7$ for Books and 0.6 for Castle in Fig. 8-9, $\lambda = 0.7$ for Books and 0.55 for Castle in Figures 10-12 regardless of q . Moreover, we also present the PSNR value of the recovered image with blurrier $q = \tilde{f}$, resulting in smallest PSNR value. However, we cannot pursue a high value of α all the time, since if \bar{g} has strong artifacts, the recovered image also tends to keep these artifacts; in Fig. 14, the recovered images with $q = \bar{g}$, $\alpha = 10$, give higher PSNR as well as better visual quality than the one with higher $\alpha = 20$, with the same $\lambda = 8$. By the same reason, the recovered image

with $q = \bar{f}$ can provide even better visual quality than the one with $q = \bar{g}$; in Fig. 14, the recovered image with $q = \bar{f}$ gives the best visual quality, providing clearer texture (left bottom part) and less artifacts near mouth, even though the PSNR value is slightly smaller.

In Fig. 15, we test the models with different number of frames $k = 1, 3, 5, 7, 10, 15, 20, 25, 30$ using the degraded images from Fig. 13. In all the cases, we fix the parameters $\lambda = 10$ for Multiframe/RO model (4), and $\lambda = 12$ for Multiframe/NLTV model (5). First, we observe that the PSNR values of \bar{f} seem to increase slightly as k increases (despite of an exception at $k = 25$), while the ones of the recovered images using both multiframe models increase with large amount, especially until $k = 7$. This means that even slight change of \bar{f} induces big improvement of the recovered image. Additionally, we present the recovered image using Multiframe/NLTV model from 30 frames, with much less artifacts both near the mouth and on the hand, and very well recovered texture part.

Furthermore, in Fig. 17, we present recovery of real color videos (fps=25) degraded by varying noisy blur kernels of type A or type B. We generate data using the pill-box kernel K of support 21×21 with radius $r = 1.5$, $s_k \sim N(0, 6^2)$, and n_k with noise density $d = 0.002$. We use 25 data frames for \bar{f} , and we present the results of Lucy-Richardson method with \bar{f} , Multiframe/RO model, and Multiframe/NLTV model with $q = \bar{f}$. Both multiframe models provide cleaner images and higher PSNR values than Lucy-Richardson method, and again Multiframe/NLTV model gives better results by providing cleaner image, especially edge parts, and higher PSNR than Multiframe/RO model. Additionally, we present the PSNR values of \bar{f} , \bar{g} , recovered images using Multiframe/RO and Multiframe/NLTV model, at every second, i.e. using 25 frames per second. Note that the videos can be found on the website: <http://www.math.ucla.edu/~gomtaeng/research.html>.

Lastly, Fig. 16 shows a successful segmentation and restoration from a severely degraded image by a noisy blur kernel. As seen in (d) in the top row, one frame method fails to find the object boundary. But, the proposed multiframe model (6) gives smooth curve evolution, leading to successful object detection as well as good restoration of image u , which can be seen in the middle and bottom rows. Here we generate 25 data frames using Gaussian kernel K of support 22×22 with $\sigma_b = 1$, $s_k \sim N(0, 10^2)$, and $n_k \sim N(0, 10^2)$.

For the computational time, e.g., in Multiframe/NLTV model with the multichannel case, it takes about 5 minutes for constructing the weight function of a 256×256 color image with the 11×11 search window and 5×5 patch in MATLAB on a dual core laptop with 2GHz processor and 2GB memory. Once we have constructed the weight, the minimization for u based on the gradient descent method takes about 50 seconds to compute 500 iterations.

4 Summary and Conclusions

We introduced a new degradation model with a noisy blur kernel, providing two different types of degradations such as perturbations or severe noise. We consider

the image restoration problem within the variational framework, by formulating the minimization problems called Multiframe/RO and Multiframe/NLTV; we assume that multiple noisy-blurry data are given with the same noise variance for the noise in the blur kernel. Both models give satisfactory results visually as well as according to PSNR. In addition, Multiframe/NLTV model incorporating nonlocal regularizer, well-known for texture denoising, provides better results than Multiframe/RO model. However, we also have a limitation, in the sense that we need more than one frame to ensure satisfactory recovery. As seen in Fig. 2, we would obtain very good results from one frame when s is known. Applications to color images, real videos, and binary image segmentation are also illustrated.

References

1. M.R. Bhatt, U.B. Desai, "Robust Image Restoration Algorithm Using Markov Random Field Model", *CVGIP: Graphical Models and Image Processing* 56(1): 61-74, 1994.
2. M. Bilgen, H.S. Hung, "Restoration of noisy images blurred by a random point spread function", *IEEE Int. Symp. on Circuits and Systems* 1: 759-762, 1990.
3. M. Bilgen, W.H. Brockman, "Restoration of noisy images blurred by a random medium", 1992.
4. M. Bilgen, H.S. Hung, "Constrained least-squares filtering for noisy images blurred by random point spread function", *Opt. Eng.* 33(6): 2020-2023, 1994.
5. P. Blomgren, T.F. Chan, "Color TV: Total variation methods for restoration of vector-valued images", *IEEE TIP* 7(3): 304-309, 1998.
6. N.K. Bose, M.K. Ng, A.C. Yau, "A fast algorithm for image super-resolution from blurred observations", *EURASIP J. Applied Sign. Proc.* 1-14, 2006.
7. A. Brook, R. Kimmel, N. Sochen, "Variational restoration and edge detection for color images", *J. Math. Imag. Vis.*, vol. 18, pp. 247-268, 2003.
8. A. Buades, B. Coll, J.M. Morel, "A review of image denoising algorithms, with a new one", *SIAM MMS* 4(2): 490-530, 2005.
9. T.F. Chan, L.A. Vese, "Active contours without edges", *IEEE TIP* 10(2): 266-177, 2001.
10. T.F. Chan, C.K. Wong, "Total variation blind deconvolution", *IEEE TIP* 7(3): 370-375, 1998.
11. P.L. Combettes, H.J. Trussell, "Methods for Digital Restoration of Signals Degraded by a Stochastic Impulse Response", *IEEE Trans. Acoustics, Speech and Signal Processing* 37: 393-401, 1989.
12. A. Efros, T. Leung, "Texture synthesis by non-parametric sampling", *ICCV*, 1999.
13. S. Farsiu, D. Robinson, M. Elad, P. Milanfar, "Fast and Robust Multi-frame Super-resolution", *IEEE TIP* 13(10): 1327-1344, 2004.
14. S. Geman, D. Geman, "Stochastic relaxation, Gibbs distributions, and the Bayesian restoration of images", *IEEE TPAMI* 6: 721-741, 1984.
15. D. Geman, G. Reynolds, "Constrained Restoration and the Recovery of Discontinuities", *IEEE T on PAMI*, Vol. 14, No. 3, 1992.
16. G. Gilboa, S. Osher, "Nonlocal linear image regularization and supervised segmentation", *SIAM MMS* 6(2): 595-630, 2007.
17. G. Gilboa, S. Osher, "Nonlocal operators with applications to image processing", *SIAM MMS* 7(3): 1005-1028, 2008.

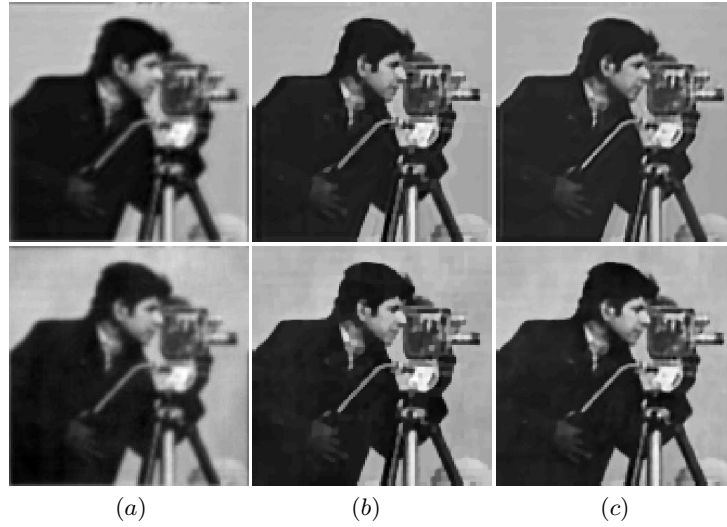


Fig. 4. TV-mean \bar{f} and recovered images with multiframe models. Top: (a) \bar{f} from 10 data frames with one frame shown in Fig. 1 top (d); recovered images using (b) Multiframe/RO, (c) Multiframe/NLTV. Bottom: (a) \bar{f} from 10 data frames with one frame shown in Fig. 1 bottom (d); recovered images using (b) Multiframe/RO, (c) Multiframe/NLTV. PSNR: top (a) 22.4973, (b) 26.8390, (c) 27.1252, bottom (a) 22.6994, (b) 26.8036, (c) 27.1490.



Fig. 5. Recovered images with multiframe models. Top: (a) original image, (b) degraded image (one frame) $f = (K + s) * u$ with the given $K + s$ in bottom (a) in Fig. 1, (c) recovered image using RO model with the unknown s and one frame. Bottom: (a) \bar{f} from 10 data frames, recovered images using (b) Multiframe/RO, (c) Multiframe/NLTV. PSNR: top (b) 22.1770, (c) 22.8667, bottom (a) \bar{f} : 22.9172, (b) 24.2993, (c) 25.8226.

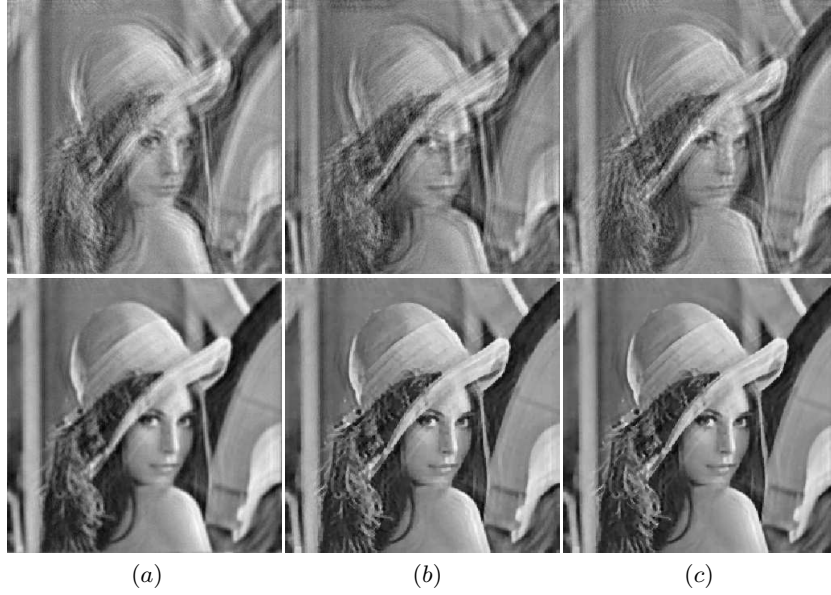


Fig. 6. Top: degraded images $f_k = (K + s_k) * u + n_k$, $k = 1, 2, 3$ (out of 10 data frames), with the pill-box kernel K of support 31×31 and radius $r = 2$, $s_k \sim N(0, 5^2)$ and $n_k \sim N(0, 5^2)$. Bottom: (a) $\bar{f} = \sum_{k=1}^{10} \mu_k f_k$ from the top row, recovered images using (b) Multiframe/RO, (c) Multiframe/NLTV. PSNR: top (a) 20.2258, (b) 17.5298, (c) 21.2778, bottom (a) \bar{f} : 25.4886, (b) 28.3715, (c) 28.9649.

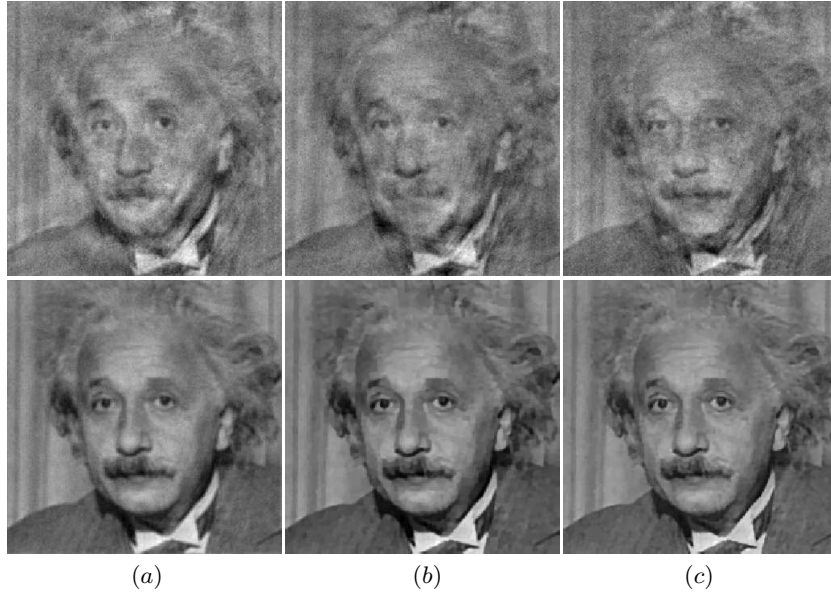


Fig. 7. Top: degraded images $f_k = (K + s_k) * u + n_k$, $k = 1, 2, 3$ (out of 10 data frames), with the pill-box kernel K of support 71×71 and radius $r = 2$, $s_k \sim N(0, 2^2)$ and $n_k \sim N(0, 10^2)$. Bottom: (a) $\bar{f} = \sum_{k=1}^{10} \mu_k f_k$ from the top row, recovered images using (b) Multiframe/RO, (c) Multiframe/NLTV. PSNR: top (a) 21.4679, (b) 21.3775, (c) 22.4948, bottom (a) \bar{f} : 28.3977, (b) 30.7696, (c) 31.1031.



Fig. 8. (A) Top: (a) original image, (b) degraded image (one frame) $f = (K + s) * u + n$ with the same $(K + s)$ in Fig. 3 (a) and noise density $d = 0.001$, (c) \bar{f} from 10 data frames. Bottom: (a) \bar{g} with $\alpha = 15$, recovered images using (b) Multiframe/RO, (c) Multiframe/NLTV with $q = \bar{g}$. PSNR: top (b) f : 16.1659, (c) \bar{f} : 18.6177, bottom (a) 21.0103, (b) 20.5248, (c) 20.8851.

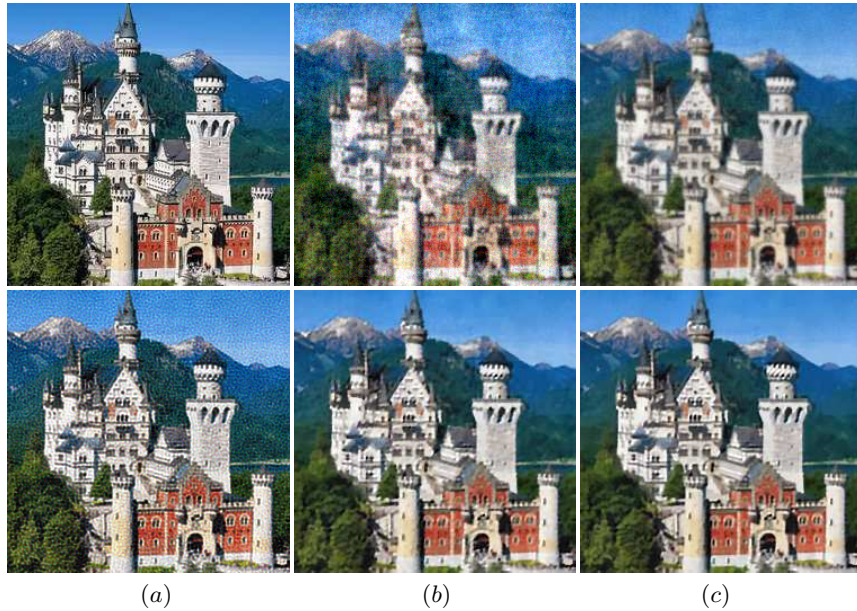


Fig. 9. (A) Top: (a) original image, (b) degraded image (one frame) $f = (K + s) * u + n$ with the same $(K + s)$ in Fig. 3 (c) and noise density $d = 0.005$, (c) \bar{f} from 10 data frames. Bottom: (a) \bar{g} with $\alpha = 15$, recovered images using (b) Multiframe/RO, (c) Multiframe/NLTV with $q = \bar{g}$. PSNR: top (b) f : 17.0298, (c) \bar{f} : 19.5645, bottom (a) 21.6415, (b) 20.8484, (c) 21.2591.

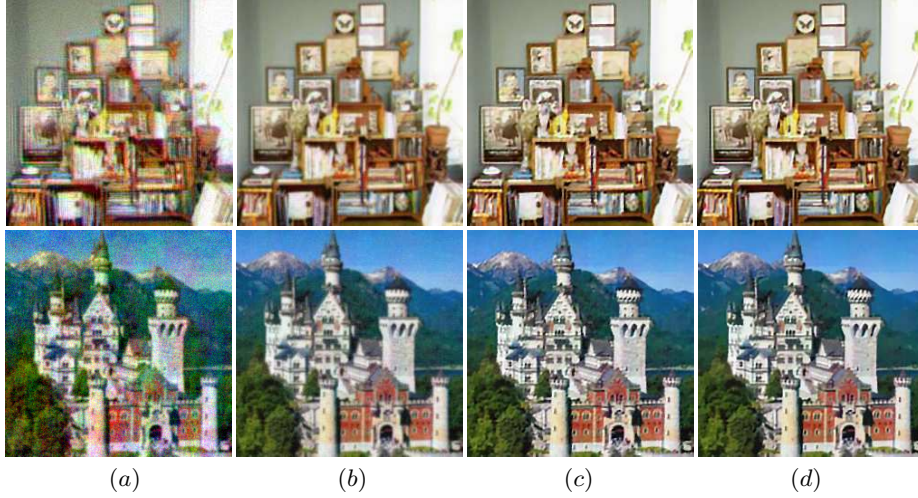


Fig. 10. (B) (a) degraded image (one frame) $f = (K + s) * u + n$ (top) with the same $(K + s)$ in Fig. 3 (b) and noise density $d = 0.001$, (bottom) with the same $(K + s)$ in Fig. 3 (d) and noise density $d = 0.005$, (b) \bar{f} from 10 data frames, recovered images using (c) Multiframe/RO, (d) Multiframe/NLTV with $q = \bar{q}$ and $\alpha = 15$. PSNR: top (a) 17.1705, (b) \bar{f} : 18.7907, (c) 20.4440, (d) 20.5432, bottom (a) 16.7133, (b) \bar{f} : 19.5224, (c) 20.9269, (d) 21.2115.

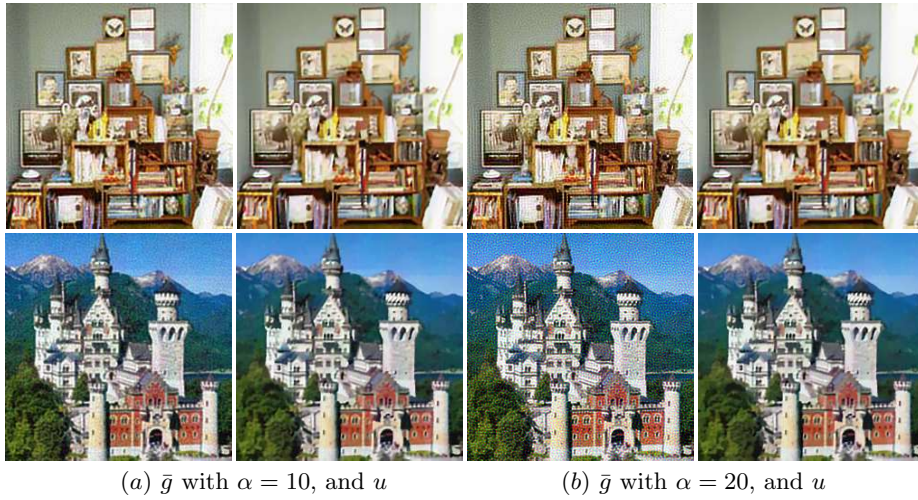


Fig. 11. Recovered images u using Multiframe/NLTV with different α for $q = \bar{q}$ with the given data (a) in Fig. 10. 1st, 3rd column: \bar{g} with $\alpha = 10$ and $\alpha = 20$ respectively. 2nd, 4th column: recovered images with the corresponding $q = \bar{q}$.

RECOVERED IMAGE u WITH DIFFERENT WEIGHT FUNCTION w_q (SAME OPTIMAL λ)					
q	\bar{g} with $\alpha = 7$	$\alpha = 10$	$\alpha = 15$	$\alpha = 20$	mean \bar{f}
Books (B)	PSNR(u)= 20.3648	20.4544	20.5432	20.5727	20.2725
Castle (B)	PSNR(u)= 21.0196	21.1282	21.2115	21.2192	20.8830

Fig. 12. Comparison of the recovered image u from the degraded images (a) in Fig. 10 using Multiframe/NLTV with different weight function w_q . $\lambda = 0.7$ for Books, 0.55 for Castle.



Fig. 13. (A) Top: (a) original image, (b)-(d) degraded images $f_k = (K + s_k) * u$, $k = 1, 2, 3$ (out of 10 data frames), with the pill-box kernel K of support 71×71 and radius $r = 2.5$, $s_k \sim N(0, 0.8^2)$. Bottom: (a) \bar{f} from 10 data frames, (b) recovered image using Multiframe/RO, (c) \bar{g} with $\alpha = 10$, (d) \bar{g} with $\alpha = 20$. PSNR: top (b) 21.4318, (c) 20.9718, (d) 21.1142, bottom (a) \bar{f} : 22.1743, (b) 26.5147, (c) 24.9449, (d) 26.2488.



Fig. 14. Recovered images using Multiframe/NLTV with (a) $q = \bar{f}$, (b) $q = \bar{g}$ with $\alpha = 10$, (c) $q = \bar{g}$ with $\alpha = 20$ in Fig. 13. PSNR: (a) 27.1031 ($\lambda = 11$), (b) 27.1758 ($\lambda = 8$), (c) 27.1223 ($\lambda = 8$).

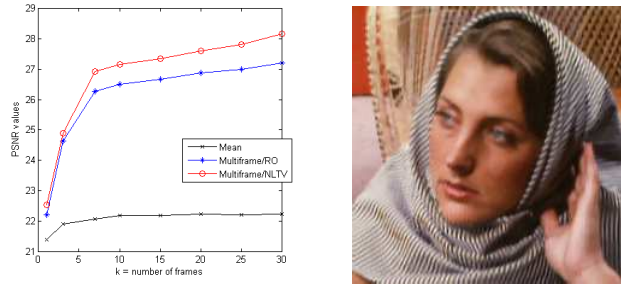


Fig. 15. Graph of PSNR versus the number of frames k used (using the degraded images in Fig. 13). (a) PSNR values of \tilde{f} , recovered image using Multiframe/RO (fixed $\lambda = 10$), Multiframe/NLTV with $q = \tilde{f}$ (fixed $\lambda = 12$) vs k , (b) recovered image using Multiframe/NLTV with $k = 30$ with optimal $\lambda = 20$: PSNR=29.1959.

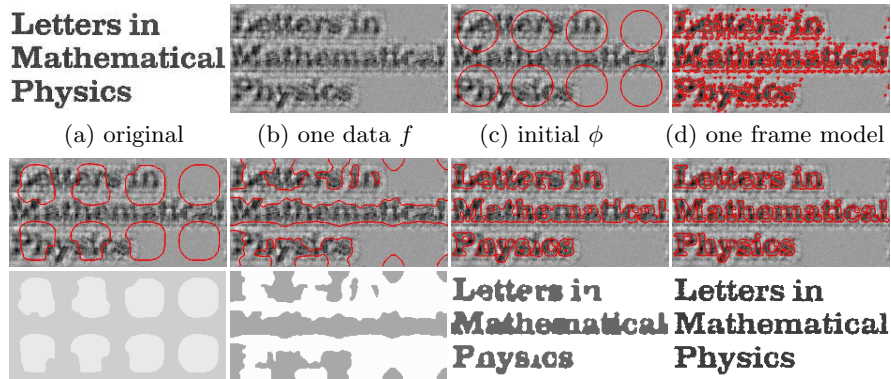
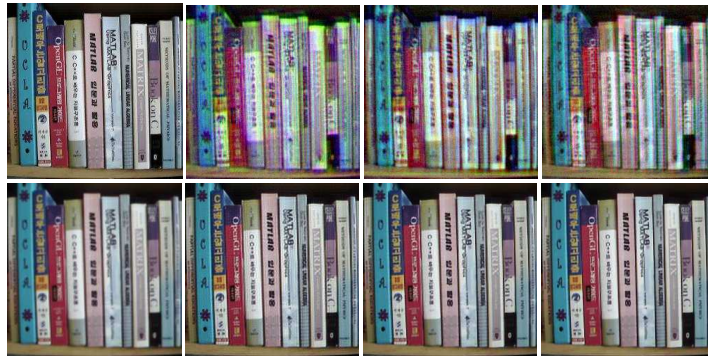


Fig. 16. Segmentation of a binary image degraded by a noisy blur kernel. Top: (d) final curve (zero level set of ϕ) with one data f . Middle, Bottom: segmentation using 25 data frames, curve evolution (middle), and the corresponding recovered images $u = c_1 H(\phi) + c_2(1 - H(\phi))$ (bottom) at the iterations 200, 300, 500, 900 with $\lambda = 55 \cdot 255^2$.

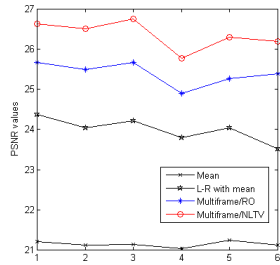
TYPE.A.



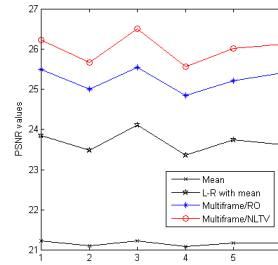
TYPE.B.



(a) (b) (c) (d)



TYPE.A.



TYPE.B.

Fig. 17. Real video restoration of type A (1st, 2nd row) and B (3rd, 4th row). Top (1st, 3rd row): (a) one original sequence, (b)-(d) degraded sequences (out of 25 data frames). Bottom (2nd, 4th row): (a) $\bar{f} = \sum_{k=1}^{25} f_k$ from the corresponding top row, (b) \bar{g} with $\alpha = 10$, recovered image using (c) Multiframe/RO and (d) Multiframe/NLTV with $q = \bar{f}$. 5th row: plots of PSNR values of \bar{f} , \bar{g} , recovered images using Multiframe/RO and Multiframe/NLTV model, at every second, i.e. using 25 frames per second. PSNR of type A: top (b) 17.3221, (c) 16.5711, (d) 18.0077, bottom (a) \bar{f} : 21.1275, (b) 24.2129, (c) 25.6732, (d) 26.7694. PSNR of type B: top (b) 16.8509, (c) 17.1406, (d) 17.0949, bottom (a) \bar{f} : 21.2134, (b) 24.1186, (c) 25.5584, (d) 26.5092. Note that videos are given on the website: <http://www.math.ucla.edu/~gomtaeng/research.html>.

18. R.C. Gonzalez, R.E. Woods, "Digital Image Processing", 3rd edition, Prentice-Hall, 2008.
19. L. Guan, R.K. Ward, "Restoration of stochastically blurred images by the geometrical mean filter", *Opt. Eng.* 29, 289-295, 1990.
20. M.L. Hambaba, "Robust deblurring of random blur", *Applied Optics*, 33(14): 2877-2882, 1994.
21. L. He, A. Marquina, S.J. Osher, "Blind deconvolution using TV regularization and Bregman iteration", *Int. J. Imaging Syst. Technol.*, Vol. 15, pp. 74-83, 2005.
22. B.R. Hunt, "The application of constrained least squares estimation to image restoration by digital computer", *IEEE Trans. Comput.* 22, 805-812, 1973.
23. M. Jung, G. Chung, G. Sundaramoorthi, L.A. Vese, A.L. Yuille, "Sobolev gradients and joint variational image segmentation, denoising and deblurring", *SPIE proceedings on Electronic Imaging*, 2009.
24. M. Jung, A. Marquina, L.A. Vese, "Multiframe Image Restoration in the Presence of Noisy Blur Kernel", to appear, *ICIP* 2009.
25. S. Kindermann, S. Osher, P.W. Jones, "Deblurring and denoising of images by nonlocal functionals", *SIAM MMS* 4(4): 1091-1115, 2005.
26. Y. Lou, X. Zhang, S. Osher, A. Bertozzi, "Image recovery via nonlocal operators", *Journal of Scientific Computing* (to appear), 2009.
27. L.B. Lucy, "An iterative technique for the rectification of observed distributions", *Astronomical Journal* 79(6): 745-754, 1974.
28. A. Marquina, S. Osher, "Image Super-Resolution by TV-Regularization and Bregman Iteration", *JSC* 37(3): 367-382, 2008.
29. A. Marquina, "Nonlinear Inverse Scale Space Methods for Total Variation Blind Deconvolution", *SIAM J. on Imaging Sci.*, vol. 2, pp. 64-83, 2009.
30. V.Z. Mesarovic, N.P. Galatsanos, A.K. Katsaggelos, "Regularized constrained total least-squares image restoration", *IEEE TIP* 4(8): 1096-1108, 1995.
31. S. Osher, R. Fedkiw, "Level set methods and dynamic implicit surfaces", Springer, New York, 2003.
32. M. Protter, M. Elad, H. Takeda, P. Milanfar, "Generalizing the Non-Local-Means to Super-resolution Reconstruction", *IEEE TIP* 18(1): 36-51, 2009.
33. D. Rajan, S. Chaudhuri, "Simultaneous estimation of super-resolved scene and depth map from low resolution defocused observations", *IEEE TPAMI* 25(9): 1102-1117, 2003.
34. W. H. Richardson, "Bayesian-Based Iterative Method of Image Restoration", *JOSA* 62 (1): 55-59, 1972.
35. L. Rudin, S. Osher, E. Fatemi, "Nonlinear Total Variation Based Noise Removal Algorithms", *Physica D* 60: 259-268, 1992.
36. L. Rudin, S. Osher, "Total variation based image restoration with free local constraints", *IEEE ICIP*, vol. I, 1994. Austin, TX.
37. J.A. Sethian, "Level Set Methods and Fast Marching Methods Evolving Interfaces in Computational Geometry, Fluid Mechanics, Computer Vision, and Materials Science", Cambridge University Press, 1999.
38. D. Slepian, "Linear least squares filtering of distorted images", *J. Opt. Soc. Am.* 57, 918-922, 1967.
39. H. Takeda, P. Milanfar, M. Protter, M. Elad, "Superresolution Without Explicit Subpixel Motion Estimation", *IEEE TIP* 18(9): 1958-1975, 2009.
40. R.K. Ward, B.E.A. Saleh, "Restoration of images distorted by systems of random impulse response", *J. Opt. Soc. Am. A* 2(8): 1254-1259, 1985.
41. R.K. Ward, B.E.A. Saleh, "Restoration of images distorted by systems of random time-varying impulse response", *J. Opt. Soc. Am. A* 3, 800-807, 1986.

42. R.K. Ward, B.E.A. Saleh, "Deblurring random blur", IEEE Trans. Acoust. Speech Sig. Proc. ASSP-34, 1494-1498, 1987.
43. L.P. Yaroslavsky, Digital image processing: An Introduction. Springer, 1985.
44. Y. You, M. Kaveh, "Blind image restoration by anisotropic regularization", IEEE Transactions on Image Processing 8:3 pp. 396-407, 1999.
45. D. Zhou, B. Scholkopf, "A Regularization Framework for Learning from Graph Data", In: Workshop on Statistical Relational Learning and Its Connections to Other Fields, 2004.